THE ASTROPHYSICAL JOURNAL LETTERS, 719:L1–L4, 2010 August 10 doi:10.1088/2041-8205/719/1/L1

OSCILLATORY MIGRATING MAGNETIC FIELDS IN HELICAL TURBULENCE IN SPHERICAL DOMAINS

DHRUBADITYA MITRA[1,2], REZA TAVAKOL[1], PETRI J. KÄPYLÄ[2,3], AND AXEL BRANDENBURG[2,4]
[1] Astronomy Unit, School of Mathematical Sciences, Queen Mary University of London, Mile End Road, London E1 4NS, UK; dhruba.mitra@gmail.com
[2] NORDITA, AlbaNova University Center, Roslagstullsbacken 23, SE-10691 Stockholm, Sweden
[3] Department of Physics, Gustaf Hällströmin katu 2a (P.O. Box 64), University of Helsinki, FI-00014 Helsinki, Finland
[4] Department of Astronomy, AlbaNova University Center, Stockholm University, SE-10691 Stockholm, Sweden
Received 2010 April 1; accepted 2010 June 21; published 2010 July 16

ABSTRACT

We present direct numerical simulations of the equations of compressible magnetohydrodynamics in a wedge-shaped spherical shell, without shear, but with random helical forcing which has negative (positive) helicity in the northern (southern) hemisphere. We find a large-scale magnetic field that is nearly uniform in the azimuthal direction and approximately antisymmetric about the equator. Furthermore, the large-scale field in each hemisphere oscillates on nearly dynamical timescales with reversals of polarity and equatorward migration. Corresponding mean-field models also show similar migratory oscillations with a frequency that is nearly independent of the magnetic Reynolds number. This mechanism may be relevant for understanding equatorward migration seen in the solar dynamo.

Key words: Sun: dynamo

Online-only material: color figures

1. INTRODUCTION

Large-scale magnetic fields with fascinating quasi-regular spatiotemporal behavior are ubiquitous in solar and stellar settings. Understanding the mechanisms for the generation of such fields and their spatiotemporal variations is still a major challenge for dynamo theory. The solar magnetic field has three particularly important features: quasi-regular oscillations, reversal of polarity, and equatorward migration. Direct numerical simulations (DNSs) of solar-like convective dynamos have been able to generate large-scale magnetic fields (Brown et al. 2007, 2010) which in some cases show oscillatory behavior, but the fields exhibit either rather weak equatorward migration at high latitudes (Ghizaru et al. 2010) or anti-solar (i.e., poleward) migration (Gilman 1983; Käpylä et al. 2010).

A useful tool for studying these dynamical phenomena is mean-field (MF) electrodynamics (e.g., Krause & Rädler 1980; Brandenburg & Subramanian 2005), where the effects of turbulence are characterized by turbulent magnetic diffusion and an α effect. According to MF theory, equatorward migration is expected if there is negative radial shear accompanied by a positive (negative) α effect in the northern (southern) hemisphere (Krause & Rädler 1980). DNSs of helical turbulence with shear have confirmed the presence of migratory dynamo waves (Brandenburg et al. 2001; Käpylä & Brandenburg 2009). It is, however, unclear whether this is really what is going on in the Sun, since there the layer with negative radial shear is rather thin and only concentrated near the surface (see, e.g., Brandenburg 2005, and references therein). The other alternative is that meridional circulation might change the direction of migration (Choudhuri et al. 1995), but evidence for this has not yet been seen in the DNS.

In this Letter, we present a completely different mechanism for polarity reversal and equatorward migration of dynamo activity. In the context of MF models, this mechanism is connected with the antisymmetry of the profiles of α across the equator (Rüdiger & Hollerbach 2004; Brandenburg et al. 2009). We demonstrate the operation of this mechanism in the DNS of the equations of magnetohydrodynamics (MHD). Our model consists of a spherical wedge-shaped shell in which the turbulence in the fluid is maintained by a random helical forcing. Motivated by the Sun, we choose our forcing to have opposite signs of helicity in the two hemispheres (negative in the north and positive in the south). We emphasize that, even though our model does not explicitly include convection, stratification, and rotation, the helical forcing used here does partially model these features implicitly.

Our model shows large-scale magnetic fields in excess of the equipartition value. More importantly, we find oscillations of the magnetic field which show opposite signs in different hemispheres with periodic reversals of polarity. Furthermore, the magnetic field develops at higher latitudes and migrates equatorward where the two different polarities of magnetic field annihilate and the cycle repeats itself as shown in the top panel of Figure 1. To our knowledge, such dynamical features of the large-scale magnetic field have not been observed earlier in the DNS of MHD turbulence. Below we introduce our model, discuss its oscillatory solutions, and briefly compare our DNS results with those obtained from the corresponding MF models.

2. THE MODEL

In our simulations, we solve the equations for compressible MHD in terms of the velocity $\boldsymbol{U}$, the logarithmic density $\ln\rho$, and the magnetic vector potential $\boldsymbol{A}$,

$$D_t\boldsymbol{U} = -c_s^2\boldsymbol{\nabla}\ln\rho + \frac{1}{\rho}\boldsymbol{J}\times\boldsymbol{B} + \boldsymbol{F}_{\rm visc} + \boldsymbol{f}, \quad (1)$$

$$D_t\ln\rho = -\boldsymbol{\nabla}\cdot\boldsymbol{U}, \quad (2)$$

$$\partial_t\boldsymbol{A} = \boldsymbol{U}\times\boldsymbol{B} + \eta\nabla^2\boldsymbol{A}, \quad (3)$$

where $\boldsymbol{F}_{\rm visc} = (\mu/\rho)(\nabla^2\boldsymbol{U} + \frac{1}{3}\boldsymbol{\nabla\nabla}\cdot\boldsymbol{U})$ is the viscous force, μ is the dynamic viscosity, $\boldsymbol{B} = \boldsymbol{\nabla}\times\boldsymbol{A}$ is the magnetic field, $\boldsymbol{J} = \boldsymbol{\nabla}\times\boldsymbol{B}/\mu_0$ is the current density, μ_0 is the vacuum permeability, c_s is the (constant) speed of sound in the medium, η is the magnetic diffusivity, and $D_t \equiv \partial_t + \boldsymbol{U}\cdot\boldsymbol{\nabla}$ is the advective derivative. Our computational domain is a spherical wedge with radius $r \in [r_1, r_2]$ symmetric about the equator

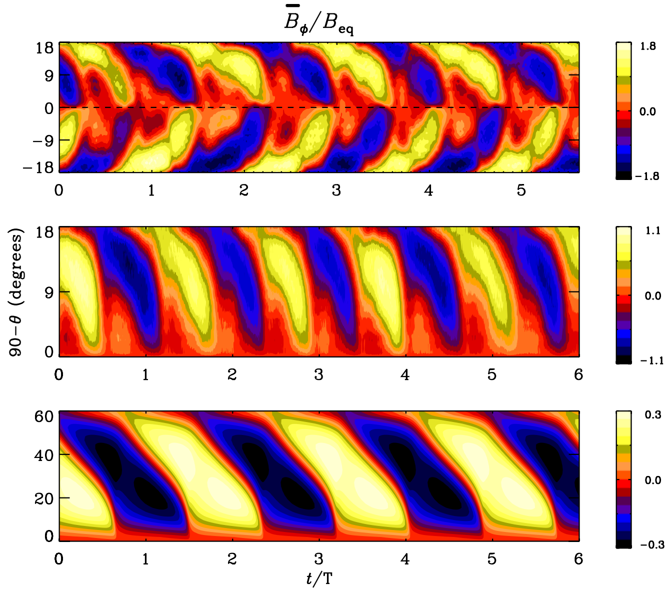

Figure 1. Space-time diagrams of the azimuthal component of the large-scale magnetic field for DNSs over both the hemispheres (top panel), DNSs over only the northern hemisphere with an antisymmetric condition at the equator (middle panel), and MF simulation over only the northern hemisphere with an antisymmetry condition at the equator (bottom panel).

(A color version of this figure is available in the online journal.)

with colatitude $\theta \in [\Theta, \pi - \Theta]$ and azimuth $\phi \in [0, \Phi]$. The radial, meridional, and azimuthal extents of our domain are, respectively, $L_r \equiv r_2 - r_1$, $L_\theta \equiv r_2(\pi - 2\Theta)$, and $L_\phi \equiv r_2\Phi$. All lengths are measured in the units of r_2. Our main results do not depend on our choices of Θ and Φ.

In Equation (1), $\boldsymbol{f}(\boldsymbol{x}, t)$ is an external white-in-time random helical forcing constructed using the Chandrasekhar–Kendall functions (Chandrasekhar & Kendall 1957) as described below. In the spherical coordinates, a helical vector function can be expressed in terms of a scalar potential function:

$$\psi\left(\beta(t), \ell(t), m(t)\right) = \mathrm{Re}\, z_\ell(\beta r) Y_\ell^m(\theta, \phi) \exp[\mathrm{i}\xi_m(t)], \quad (4)$$

with $z_\ell(\beta r) = a_\ell j_\ell(\beta r) + b_\ell n_\ell(\beta r)$. Here, j_ℓ and n_ℓ are spherical Bessel functions of the first and second kind, respectively, a_ℓ and b_ℓ are constants determined by the boundary conditions, and ξ_m is a random angle uniformly distributed between 0 and 2π. The helical forcing $\boldsymbol{f}$ is then given by the equation $\boldsymbol{\nabla} \times \boldsymbol{f} = \beta \boldsymbol{f}$, where $\boldsymbol{f} = \boldsymbol{T} + \boldsymbol{S}$, $\boldsymbol{T} = \boldsymbol{\nabla} \times (\boldsymbol{e}\psi)$, and $\boldsymbol{S} = \beta^{-1}\boldsymbol{\nabla} \times \boldsymbol{T}$, where $\boldsymbol{e}(t)$ is a unit vector chosen randomly on the unit sphere. As to the choice of boundary conditions, we demand that $\boldsymbol{f}$ is zero at the two radial boundaries $r = r_1$ and $r = r_2$ which yields the following transcendental equation relating a_ℓ, b_ℓ, and β:

$$a_\ell j_\ell(\beta r_1) + b_\ell n_\ell(\beta r_1) = a_\ell j_\ell(\beta r_2) + b_\ell n_\ell(\beta r_2) = 0. \quad (5)$$

We first construct a table of values of m, ℓ, and β in the following way. As we use periodic boundary conditions along the azimuthal direction, $m_{\min} = 2\pi/\Phi$. We choose $m = pm_{\min}$, and for a fixed m we choose ℓ to be odd, $\ell = 2(m+q)+1$, because we want the forcing to go to zero at the equator. Here, p and q are integers which range between 3 and 5. For a fixed ℓ and m, we solve Equation (5) by the Newton–Raphson method and list the solutions which have 3–5 zeros in the domain. To randomize the resulting forcing, we randomly choose a triplet of m, ℓ, and β from the table. We also randomize the unit vector $\boldsymbol{e}$ on the unit sphere. Two different signs of helicity are imposed by choosing negative (positive) β in the northern (southern) hemisphere. The choice of parameters implies that we have a scale separation between 3 and 5 in our simulations. Our results are fairly robust under the change of different parameters of forcing. We need scale separation of 3 or more to excite a large-scale dynamo (Haugen et al. 2004), which invariably shows oscillations and equatorward migration. Our simulations are performed using the Pencil Code[5]; see Mitra et al. (2009) for details regarding the implementation of the spherical polar coordinates.

We use periodic boundary conditions along the azimuthal direction and set the normal component of the magnetic field to zero on all other boundaries (perfect-conductor boundary condition). This is implemented by setting the two tangential components of $\boldsymbol{A}$ to zero. As an estimate of the characteristic Fourier mode of the forcing we define $k_\mathrm{f} = w_\mathrm{rms}/u_\mathrm{rms}$ (Column 8 of Table 1), where w_rms and u_rms are the rms values of small-scale vorticity and velocity, respectively. We introduce the fluid and magnetic Reynolds numbers as $\mathrm{Re} = u_\mathrm{rms}/\nu k_\mathrm{f}$ and $\mathrm{Re_M} = u_\mathrm{rms}/\eta k_\mathrm{f}$, respectively. Here, $\nu = \mu/\rho_0$ is the mean kinematic viscosity, where ρ_0 is the initial and the mean density in the volume. A representative list of parameters is given in Table 1.

3. RESULTS

We start our simulations with a random seed magnetic field of no particular parity about the equator. After a transient time, of about one turbulent diffusion time, we find that a large-scale magnetic field is generated with energy on the order of or exceeding the equipartition strength in all runs. The magnetic field encompasses the whole azimuthal extent of the domain. A contour plot of the toroidal component of the magnetic field on a surface with constant radius from Run S5 is shown in Figure 2. We define the large-scale magnetic field via averages over the

[5] http://pencil-code.googlecode.com

Table 1
Summary of Our Parameters Including Grid Size, the Meridional and Azimuthal Extents of Our Domain, rms Value of the Azimuthally Averaged Field, Reynolds Number Re, and Magnetic Reynolds Number $\mathrm{Re_M}$

Run	Grid	L_θ	L_ϕ	$\overline{B}_\mathrm{rms}/B_\mathrm{eq}$	Re	$\mathrm{Re_M}$	k_f/k_1	$\nu \times 10^5$	$\eta \times 10^5$	$\eta_\mathrm{t} \times 10^5$	$\omega_\mathrm{c} \times 10^3$	$T \times 10^{-3}$	t_max
S1	$32 \times 64 \times 32$	$\pi/5$	$\pi/10$	0.88	5	12	3	5	2	5.3	2.5	0.18	$\sim 10T$
S2	$64 \times 128 \times 64$	$\pi/5$	$\pi/10$	0.79	8	21	4	3	1.2	6.2	2.5	0.16	$\sim 5T$
S3	$32 \times 64 \times 64$	$\pi/5$	$\pi/5$	1.16	2	4	7	5	2	3.6	2	0.27	$\sim 10T$
S4	$64 \times 128 \times 128$	$\pi/5$	$\pi/5$	1.04	4	10	7	2	1	4.9	2.6	0.2	$\sim 5T$
S5	$64 \times 128 \times 128$	$9\pi/10$	$\pi/2$	2	6.6	13	7	2	1	4.4	–	–	$\sim T$

Notes. The forcing amplitude, $f_\mathrm{amp} = 0.2$, is chosen such that the Mach number is on the order of 0.1, making the flow essentially incompressible. t_max is the duration of each run. The run S5 has not been run long enough to accurately measure ω_c.

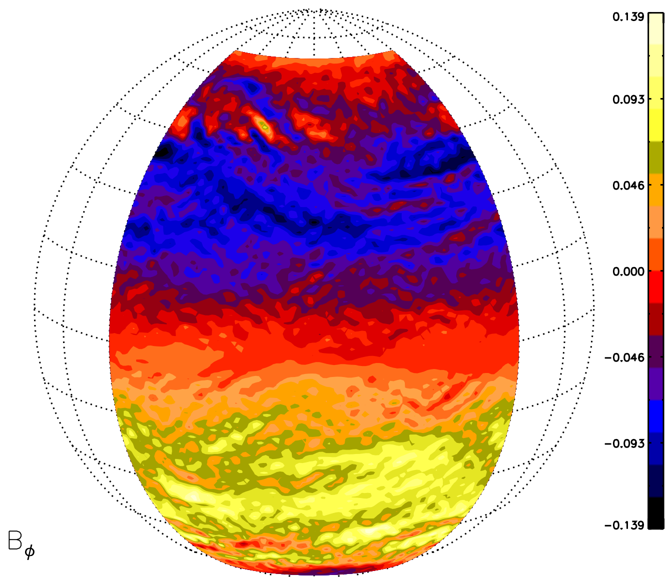

Figure 2. Orthographic projection of the toroidal magnetic field B_ϕ at $r = 0.85$ for Run S5. The projection is tilted by 15° toward the viewer.

(A color version of this figure is available in the online journal.)

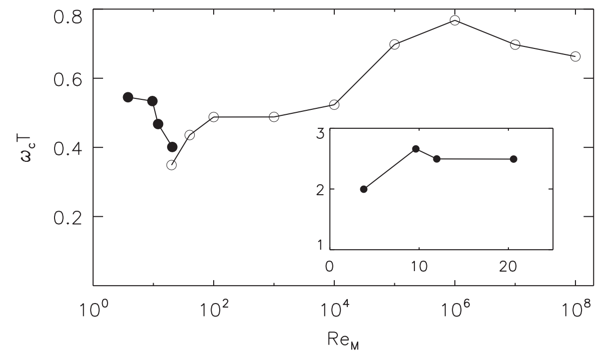

Figure 3. Frequency of the oscillations multiplied by the turbulent diffusion time $T = (\eta_t k_\theta^2)^{-1}$ as a function of $\mathrm{Re_M}$ for $L_\theta = \pi/5$. Data from DNSs (closed circles) and MF models (open circles) are shown. For the MF runs $\eta_t = 1$ and for the DNS runs η_t is given in Table 1. The inset shows $\omega_c \times 10^3$ (Table 1, Column 12) as a function of $\mathrm{Re_M}$ for the DNS data.

azimuthal and radial directions, i.e., $\overline{\boldsymbol{B}} = \langle \boldsymbol{B} \rangle_{r\phi}$, such that the resultant magnetic field is solely a function of latitude and time. We normalize the magnetic field with the equipartition field strength, $B_{\rm eq} = \langle \mu_0 \rho \boldsymbol{u}^2 \rangle^{1/2}$, where $\boldsymbol{u} = \boldsymbol{U} - \overline{\boldsymbol{U}}$ is the small-scale velocity. The field first develops at higher latitudes and then with time migrates equatorward. In each hemisphere, the field shows oscillations and reversals of polarity. These features can be seen in the space-time diagram shown in the top panel of Figure 1 where we plot $\overline{B}_\phi$ as a function of latitude and time. The principal frequency of oscillations, ω_c (Column 12 of Table 1 and the inset of Figure 3), is obtained by Fourier transforming the time series of $\overline{B}_\phi(\theta, t)$ in time at a given θ ($\theta = \pi/20$ say) and determining the frequency corresponding to the dominant mode. Normalized energy in the large-scale magnetic field also shows oscillations as a function of time, but with frequency $2\omega_c$. A characteristic dynamical timescale is the turbulent diffusion time corresponding to the length scale L_θ defined by $T \equiv (k_\theta^2 \eta_t)^{-1}$, where $k_\theta = 2\pi/L_\theta$ and for η_t we take the expression from the first-order-smoothing approximation, $\eta_t = u_{\rm rms}/3k_{\rm f}$. In all our runs, we find the product $\omega_c T$ to be of order unity (see the bottom panel of Figure 3).

We note that the radial and azimuthal components of the large-scale magnetic field are almost antisymmetric about the equator. This allows a further simplification of our model by simulating only one-half of the domain (e.g., the northern hemisphere), while keeping exactly the same forcing function (e.g., a forcing that is random, and negatively helical in the northern hemisphere going smoothly to zero at the equator), but choosing the boundary condition $B_r = B_\phi = 0$ at the equator. Such simulations produce exactly the same oscillations (as can be seen by comparing the top and the middle panels of Figure 1) as those obtained in the DNS with both hemispheres. This implies that these oscillations can be studied with half the number of grid points and appropriately chosen boundary conditions at the equator.

Given the large values of the magnetic Reynolds number in solar/stellar settings, an important question is how the frequency ω_c scales with $\mathrm{Re_M}$? This question cannot be answered from the DNS because the magnetic Reynolds numbers reached are far from the asymptotic limit of large $\mathrm{Re_M}$ (see Column 7 of Table 1). A way forward is to use analogous MF models. The appropriate setting would be that of an α^2 dynamo with dynamical α quenching (Blackman & Brandenburg 2002) which incorporates conservation of magnetic helicity, given by the equations

$$\partial_t \overline{\boldsymbol{B}} = \boldsymbol{\nabla} \times (\alpha \overline{\boldsymbol{B}}) + (\eta + \eta_t) \nabla^2 \overline{\boldsymbol{B}}, \tag{6}$$

$$\partial_t \alpha = -2\eta k_{\rm f}^2 \left(\frac{\alpha \langle \overline{\boldsymbol{B}}^2 \rangle - \eta_t \langle \overline{\boldsymbol{B}} \cdot \overline{\boldsymbol{J}} \rangle}{B_{\rm eq}^2} + \frac{\alpha - \alpha_{\rm K}}{\mathrm{Re_M}/3} \right), \tag{7}$$

where $\mathrm{Re_M}/3 = \eta_t/\eta$ and $B_{\rm eq}$ is the equipartition field strength. We use $k_{\rm f}/k_1 = 6$ in our MF simulations. In view of the discussion above, we solve the MF equations in only the northern hemisphere with appropriate boundary condition at the equator. In the MF approach, the helical nature of turbulence is modeled by the α coefficient ($\alpha_{\rm K}$). We choose $\alpha_{\rm K} = g(\theta)\alpha_0$ and $\eta_t = 1$. The profile function g takes positive (negative) values in the northern (southern) hemisphere, going smoothly to zero at the equator. This reflects the fact that, according to MF theory, the kinetic α effect usually has the opposite sign to the mean kinetic helicity. We have used three different functional forms for g, namely $g = \theta - \pi/2$, $g = \sin(\theta - \pi/2)$, and $g = \tanh(\theta - \pi/2)$, without any significant change in our results. We need $\alpha_0 \geqslant 16$ to excite a dynamo but once excited the oscillatory and migratory properties of the dynamo do not depend on α_0. We use perfect-conductor boundary conditions along the radial direction and our magnetic Reynolds number (changed by varying η) ranges between $10 \lesssim \mathrm{Re_M} \lesssim 10^8$. We have also used domains with larger latitudinal extents than those used in our DNS.

Here, we briefly mention a few important outcomes of our MF results relevant to our discussion above. (1) Our DNS results—namely oscillatory behavior as well as migration toward the equator—are qualitatively reproduced by the MF solutions in the range of parameters reported here. An example of the space-time diagram produced by our MF runs is shown in the bottom panel of Figure 1. (2) The frequency of oscillations remains almost constant as a function of $\mathrm{Re_M}$ (see Figure 3). The dependence of the oscillation period on $\mathrm{Re_M}$ seen in the DNS may be related to $\mathrm{Re_M}$ dependence of the turbulent magnetic diffusivity. A similar behavior has been observed earlier in the Cartesian DNS (Käpylä & Brandenburg 2009). (3) To show the robustness of our results with respect to the size of the domain, we also studied domain sizes extended in the meridional direction from $L_\theta = \pi/5$ to $(178/180)\pi$ which corresponds, respectively, to $\Theta = 72^\circ$ and 1°. We find that the oscillations and the migratory behavior do not change. (4) For the MF model considered here the mean value of the large-scale magnetic field decreases as $\mathrm{Re}_\mathrm{M}^{-1}$; i.e., the field is catastrophically quenched for large values of Re_M. In the DNS, however, such quenching could be alleviated by magnetic helicity fluxes across the equator (Brandenburg et al. 2009; Mitra et al. 2010).

To test the robustness of our simulations with respect to the choice of boundary condition in the radial direction, we repeated our simulations with the vertical field boundary condition, which makes the two tangential components of the magnetic field vanish at the radially outward boundary. These simulations also show oscillations and equatorward migration of magnetic activity, but in this case the oscillations are less regular and the frequency is marginally higher.

4. CONCLUSIONS

We have found large-scale fields, oscillations on dynamical timescales, and polarity reversals with equatorward migration of magnetic activity in DNSs of helically forced MHD equations in spherical wedge domains. Despite its simplicity, it is quite striking how our model can reproduce these important features of the solar dynamo. As far as we are aware, these features have not been observed earlier in the DNS. We have elucidated our DNS results by considering analogous α^2 MF models which support our conclusions. We have further used these MF models to explore magnetic Reynolds numbers that are at present inaccessible to the DNS. This has enabled us to show that the frequency of the oscillations is almost independent of Re_M for large Re_M. Such MF models have been known to have oscillatory solutions if α changes sign in the computational domain (see, e.g., Baryshnikova & Shukurov 1987; Stefani & Gerbeth 2003; Rüdiger & Hollerbach 2004; Brandenburg et al. 2009), but their migratory property had not been studied before. Antisymmetry of α with depth also produces oscillatory solutions (Baryshnikova & Shukurov 1987; Stefani & Gerbeth 2003), but not the equatorward migration.

The helical forcing used in our DNS, with its different signs of helicity in different hemispheres, implicitly models only the helical aspect of the effects of rotation and stratification present in the Sun. Physically, a more complete picture should emerge from the DNS of convective turbulent dynamo as done, for example, by Gilman (1983), Brown et al. (2007, 2010), Käpylä et al. (2010), and Ghizaru et al. (2010). Such simulations also generate differential rotation and lead to another dynamo mode of operation—the $\alpha\Omega$ dynamo—which also produces oscillatory behavior. However, in order to get equatorward migration, radial shear must be negative. Helioseismology has shown that negative radial shear exists only near the surface of the convection zone. This feature has so far not been reproduced by global DNSs. Whether or not an $\alpha\Omega$ dynamo is the dominant mechanism operating in the Sun remains unclear. It is therefore important to keep in mind that there exists alternative mechanisms for producing oscillatory behavior with equatorward migration, such as the one discussed here.

This work was supported in part by the European Research Council under the AstroDyn Research Project No. 227952 and the Swedish Research Council Grant 621-2007-4064. D.M. is supported by the Leverhulme Trust. P.J.K. is supported by the Academy of Finland grant 121431. Computational resources were granted by UKMHD, QMUL HPC facilities purchased under the SRIF initiative, the National Supercomputer Centre in Linköping in Sweden, and CSC-IT Center for Science in Espoo, Finland.

REFERENCES

Baryshnikova, I., & Shukurov, A. 1987, Astron. Nachr., 308, 89
Blackman, E., & Brandenburg, A. 2002, ApJ, 579, 359
Brandenburg, A. 2005, ApJ, 625, 539
Brandenburg, A., Bigazzi, A., & Subramanian, K. 2001, MNRAS, 325, 685
Brandenburg, A., Candelaresi, S., & Chatterjee, P. 2009, MNRAS, 398, 1414
Brandenburg, A., & Subramanian, K. 2005, Phys. Rep., 417, 1
Brown, B. P., Browning, M. K., Brun, A. S., Miesch, M. S., & Toomre, J. 2010, ApJ, 711, 424
Brown, B. P., et al. 2007, in AIP Conf. Ser. 948, Unsolved Problems in Stellar Physics: A Conference in Honor of Douglas Gough, ed. R. J. Stancliffe et al. (Melville, NY: AIP), 271
Chandrasekhar, S., & Kendall, P. 1957, ApJ, 126, 457
Choudhuri, A. R., Schüssler, M., & Dikpati, M. 1995, A&A, 303, L29
Gilman, P. A. 1983, ApJS, 53, 243
Ghizaru, M., Charbonneau, P., & Smolarkiewicz, P. K. 2010, ApJ, 715, L133
Haugen, N. E. L., Brandenburg, A., & Dobler, W. 2004, Phys. Rev. E, 70, 016308
Käpylä, P. J., & Brandenburg, A. 2009, ApJ, 699, 1059
Käpylä, P. J., Korpi, M. J., Brandenburg, A., Mitra, D., & Tavakol, R. 2010, Astron. Nachr., 331, 73
Krause, F., & Rädler, K.-H. 1980, Mean-field Magnetohydrodynamics and Dynamo Theory (Oxford: Pergamon)
Mitra, D., Candelaresi, S., Chatterjee, P., Tavakol, R., & Brandenburg, A. 2010, Astron. Nachr., 331, 130
Mitra, D., Tavakol, R., Brandenburg, A., & Moss, D. 2009, ApJ, 697, 923
Rüdiger, G., & Hollerbach, R. 2004, The Magnetic Universe: Geophysical and Astrophysical Dynamo Theory (Weinheim: Wiley-VCH)
Stefani, F., & Gerbeth, G. 2003, Phys. Rev. E, 67, 027302